International Journal of Nanomedicine

Dovepress
open access to scientific and medical research

Open Access Full Text Article

ORIGINAL RESEARCH

Enhancement of T2* Weighted MRI Imaging Sensitivity of U87MG Glioblastoma Cells Using γ-Ray Irradiated Low Molecular Weight Hyaluronic Acid-Conjugated Iron Nanoparticles

Haw-Ming Huang[1,2]
Ping-Han Wu[3]
Po-Chien Chou[4]
Wen-Tien Hsiao[5]
Hsin-Ta Wang[4]
Hsin-Pei Chiang[3]
Chi-Ming Lee[6]
Shwu-Huey Wang[6]
Yu-Cheng Hsiao[2,7]

[1]School of Dentistry, College of Oral Medicine, Taipei Medical University, Taipei, Taiwan; [2]Graduate Institute of Biomedical Optomechatronics, College of Biomedical Engineering, Taipei Medical University, Taipei, Taiwan; [3]Graduate Institute of Biomedical Materials and Tissue Engineering, College of Biomedical Engineering, Taipei Medical University, Taipei, Taiwan; [4]School of Organic and Polymeric, National Taipei University of Technology, Taipei, Taiwan; [5]Department of Medical Imaging and Radiological Technology, Yuanpei University of Medical Technology, Hsinchu, Taiwan; [6]Core Facility Center, Office of Research and Development, Taipei Medical University, Taipei, Taiwan; [7]Cell Physiology and Molecular Image Research Center, Taipei Municipal Wan Fang Hospital, Taipei Medical University, Taipei, Taiwan

Correspondence: Yu-Cheng Hsiao; Ping-Han Wu
Taipei Medical University, No. 250, Wu-Hsing Street, Taipei, 11031, Taiwan
Tel +886-291-937-9783
Fax +886 2 27362295
Email ychsiao@tmu.edu.tw; gahwclbjwph@gmail.com

Introduction: It has been reported that low-molecular-weight hyaluronic acid (LMWHA) exhibits a potentially beneficial effect on cancer therapy through targeting of CD44 receptors on tumor cell surfaces. However, its applicability towards tumor detection is still unclear. In this regard, LMWHA-conjugated iron (Fe_3O_4) nanoparticles (LMWHA-IONPs) were prepared in order to evaluate its application for enhancing the T2* weighted MRI imaging sensitivity for tumor detection.

Methods: LMWHA and Fe_3O_4 NPs were produced using γ-ray irradiation and chemical co-precipitation methods, respectively. First, LMWHA-conjugated FITC was prepared to confirm the ability of LMWHA to target U87MG cells using fluorescence microscopy. The hydrodynamic size distribution and dispersion of the IONPs and prepared LMWHA-IONPs were analyzed using dynamic light scattering (DLS). In addition, cell viability assays were performed to examine the biocompatibility of LMWHA and LMWHA-IONPs toward U87MG human glioblastoma and NIH3T3 fibroblast cell lines. The ability of LMWHA-IONPs to target tumor cells was confirmed by detecting iron (Fe) ion content using the thiocyanate method. Finally, time-of-flight secondary ion mass spectrometry (TOF-SIMS) imaging and in vitro magnetic resonance imaging (MRI) were performed to confirm the contrast enhancement effect of LMWHA-IONPs.

Results: Florescence analysis results showed that LMWHA-FITC successfully targeted the surfaces of both tested cell types. The ability of LMWHA to target U87MG cells was higher than for NIH3T3 cells. Cell viability experiments showed that the fabricated LMWHA-IONPs possessed good biocompatibility for both cell lines. After co-culturing test cells with the LMWHA-IONPs, detected Fe ion content in the U87MG cells was much higher than that of the NIH3T3 cells in both thiocyanate assays and TOF-SIMs images. Finally, the addition of LMWHA-IONPs to the U87MG cells resulted in an obvious improvement in T2* weighted MR image contrast compared to control NIH3T3 cells.

Discussion: Overall, the present results suggest that LMWHA-IONPs fabricated in this study provide an effective MRI contrast agent for improving the diagnosis of early stage glioblastoma in MRI examinations.

Keywords: hyaluronic acid, Fe_3O_4 nanoparticles, TOF-SIMS, MRI

Introduction

Clinically, there exists about a 35% chance that contrast agents will be needed to improve the image sensitivity of magnetic resonance imaging (MRI) examinations in order to improve the diagnosis accuracy for tumors and other diseases.[1] Contrast

Received: 20 February 2021
Accepted: 17 May 2021
Published: 1 June 2021

agents used for MRI can be broadly divided into two main types: T1 and T2.[2,3] T1 contrast agents change the T1 relaxation time of the tissue, and thus increase image contrast by strengthening the signal. Hence, T1 contrast agents are often referred to as positive contrast agents. On the other hand, T2 contrast agents (usually referred to as negative contrast agents) alter the T2 relaxation time and relaxivity of the tissue; thereby weakening the signal of diseased tissue and increasing the contrast with surrounding normal tissue as a result.[4] Since the T2 relaxation time of abnormal tissues is longer than that of normal tissues, T2 weighted images are generally used to diagnose inflammation and/or tumor tissue.[5] However, several common MRI contrast agents, including Gd-based compounds and high-dose Mn^{2+}, have been reported to induce undesirable side effects in some patients and to have cellular toxicity.[6,7]

T2 contrast agents usually have the form of superparamagnetic materials. Among these materials, magnetite (ferrous-ferric oxide, Fe_3O_4) and maghemite (ferrous oxide, Fe_2O_3) have attracted particular attention.[3,4,8,9] Since, for diameters less than 30 nm, they not only exhibit superparamagnetic properties but also have excellent biocompatibility and magnetic susceptibility.[10] Furthermore, through appropriate surface modification, iron oxide nanoparticles (IONPs) can be made to target specific ligands on the cell membrane.[11–13] Therefore, they have many potential applications in medicine, including hyperthermia treatment,[14–17] drug delivery,[3,9,18] biochemical sensing,[9] tissue repair,[19] and MRI sensitivity enhancement.[3,4,9] In such applications, the surfaces of IONPs are generally modified using a suitable material in order to enhance their stability and biocompatibility.[9,13,15,18]

Hyaluronic acid (HA) is widely distributed in the connective, epidermal and nerve tissues in the human body and is the main component of the extracellular matrix.[18–20] The physical and biological properties of HA depend on its molecular weight and concentration in aqueous solution. In general, the molecular weight of natural HA varies widely from 2 kDa (HA oligomers) to 10 MDa (high-molecular weight HA, HMWHA).[21–23] HMWHA has good moisture absorption capability, and thus has excellent moisturizing and viscoelastic properties. As a result, it is used extensively in medical applications for osteoarthritis treatment and wound repair.[24] HA also has a high specific-binding ability for CD44,[25–28] a marker found in abundance on the surface of cancer cells. Consequently, the feasibility for modifying the surface of IONPs with HA to enhance their ability to target cancerous tissue has attracted significant attention.[29,30]

HMWHA can be broken down into low molecular weight hyaluronic acid (LMWHA) in vivo.[31] Several recent studies have investigated the correlation between the molecular weight of HA and its physiological function.[32,33] In general, results have shown that depolymerized HA fragments have positive effects on wound healing, immune response and angiogenesis.[22,34,35] Accordingly, the problem of depolymerizing HMWHA into LMWHA fragments has attracted great interest in recent years. The methods proposed thus far for decomposing HMWHA can be broadly classified as either chemical or physical methods. However, the reaction products produced in chemical methods have the disadvantage of an inhomogeneous molecular weight (MW) distribution. In practice, the cellular targeting efficiency of HA depends strongly on the MW, and thus HA's biological effects also vary widely depending on MW.[28] A similar tendency is also observed when HA is used to modify nanoparticles.[36] Moreover, when using chemical methods to decompose HMWHA, it is difficult to precisely control the breakdown point on the long chain of HA molecules.[35] Thus, if the chemical reaction disturbs the structure related to the targeting site of CD44, for example, the biological effect of the treated HA molecules is significantly reduced.

Besides the chemical methods described above, several physical methods for depolymerizing HMWHA into LMWHA have also been proposed, including ultrasonic agitation,[37] thermal treatment[38] and γ-ray irradiation.[35,39] Among these methods, γ-ray irradiation is particularly effective in producing LMWHA with excellent wound healing properties.[35] A previous report has indicated that HA-functionalization improved the hydrophilicity, biocompatibility, and chemical/structural stability of the NP and results in high cell capture ability.[40] In vivo animal experiments have shown that HA-IONPs are more efficient than commercially available agents in enhancing the contrast of MR images.[41,42] However, there is no evidence as of yet to show that LMWHA prepared using γ-ray irradiation can also be used to modify nano-Fe_3O4 as a contrast agent for MR imaging. Accordingly, the present study produces LMWHA by γ-ray irradiation, then modifies the LMWHA with fluorescent dye and Fe_3O_4 nanoparticles (IONPs) for further investigation and experimentation. The applicability of LMWHA-IONPs for MR image enhancement is evaluated by fluorescence

microscopy, single ion mass spectrometry and T2* weighted MRI images.

Materials and Methods

Materials

$FeCl_2$•$4H_2O$ was purchased from Avantor Performance Material, Inc. (PA, USA). $FeCl_3$•$6H_2O$, toluene, ammonium persulfate, potassium thiocyanate, 1-Ethyl-3-(3-dimethylaminopropyl) carbodiimide, ethylenediamine and oleic acid were purchased from Nacalai Tesque (Kyoto, Japan). Hyaluronic acid (molecular weight 3000 kDa) was purchased from Cheng-Yi Chemical Industry Co. Ltd. (Taipei, Taiwan). NIH3T3 and U87MG cell lines were purchased from the Bioresource Collection and Research Center, Food Industry Research and Development Institute (Hsinchu, Taiwan). Fluorescein-5-isothiocyanate (FITC) and 4,6-diamidino-2-phenylindole (DAPI) was obtained from Molecular Probes, Inc. (Eugene, OR, USA). DMEM, fetal bovine serum, and penicillin-streptomycin were purchased from Gibco (Grand Island, NY, USA). Dimethyl sulfoxide (DMSO), Triton X-100, 3-(4,5-Dimethylthiazol-2-yl)-2,5-diphenyltetrazolium bromide (MTT), and agarose were obtained from Sigma-Aldrich (St. Louis, MO, USA). All other analytical-grade reagents and solvents used were purchased from J.T. Baker (NJ, USA).

Preparation of Oleic-Acid Coated Fe_3O_4 Nanoparticles

Fe_3O_4 nanoparticles were prepared using a co-precipitation method. Briefly, $FeCl_2$•$4H_2O$ and $FeCl_3$•$6H_2O$ were dissolved in an NH_4OH solution in a ratio of 1:3 and then stirred for 30 minutes. The solution was heated at 85°C for 15 minutes and then allowed to cool to room temperature, resulting in the spontaneous precipitation of IONPs.[43] The IONPs were coated with oleic acid (OA) as described in a previous report[43] and separated from the solution using a strong magnet (Figure 1A). The isolated OA-IONPs were washed with pure water and dried in an oven overnight. The dispersibility and particle size distribution of the OA-IONPs were examined using a transmission electron microscope (TEM, H-600, Hitachi, Ltd., Tokyo, Japan) and an electrophoretic light scattering device (NanoBrook 90Plus Zeta, Brookhaven Instruments, NY, USA), respectively.

Preparation of LMWHA-Fe_3O_4 NPs and FITC-Labeled LMWHA

LMWHA (200 kDa, Figure 1B) was prepared by exposing commercial HMWHA (3000 kDa) to a cobalt-60 irradiator (Point Source, AECL, IR-79, Nordion, Canada) with a dose of 1 kGy/h for 20 hours at room temperature.[35] LMWHA-IONPs were then prepared by mixing OA-IONPs (in toluene) and LMWHA (in 1N NaOH) under vigorous stirring for 24 hours. Once the OA coating on the IONPs was replaced by LMWHA, the LMWHA-IONP sample was collected via ultra-filtration and centrifugation (8000 rpm for 10 minutes) (Figure 1C). The pH of the collected LMWHA-IONPs was adjusted to 7 via the addition of 0.1 N HCl solution and the NPs were then freeze dried and placed into storage (Figure 1D).

FITC-labeled LMWHA was prepared by dissolving 2.5 mg fluorescein-5-isothiocyanate (FITC) in 20 mL of dimethyl sulfoxide (DMSO). A 2 μL of ethylenediamine solution was added to the sample and the solution was stirred for 3 hours. The LMWHA activation solution was prepared by mixing 250 mg of LMWHA solution with 0.125 g of 1-Ethyl-3-(3-dimethylaminopropyl) carbodiimide in 50 mL ultrapure water. The FITC and ethylenediamine solution was slowly dropped into the LMWHA activation solution and vigorously stirred for 48 hours to prompt a reaction. Finally, FITC-labeled LMWHA was obtained using a dialysis procedure (8000 mol units) for 48 hours. The product was then freeze dried and placed into storage for subsequent experimentation.

In vitro Cell Experiments

Targeting Ability of FITC-Labeled LMWHA

The targeting ability of LMWHA was evaluated using normal fibroblast (NIH3T3) and glioblastoma (U87MG) cell lines. Cells were seeded onto Petri dishes at a density of 1×10^4 cells/mL then incubated with Dulbecco's modified eagle medium (DMEM) supplemented with 10% fetal bovine serum (FBS) and 1% penicillin-streptomycin at 37°C with a 5% CO_2 supplement. Cells with various densities (1×10^4, 5×10^4, 1×10^5 and 5×10^5 cells/mL) were then further incubated with FITC-labeled LMWHA at concentrations of 0, 0.5, 1, 2 and 4 mg/mL for 30 minutes at 4°C. After labeling, cells were washed twice with PBS and the corresponding fluorescence intensity was detected using a multi-label plate reader (Plate Chameleon Multi-label Detection Platform, Hidex Oy, Turku, Finland) with excitation and emission wavelengths of 488 nm and 518 nm, respectively.

The ability targeting of FITC-labeled LMWHA was also examined by means of fluorescence imaging. Briefly, NIH3T3 and U87MG cells were cultured on cover glasses until full confluence. Cells were then co-cultured with FITC-labeled LMWHA and fixed with 4%

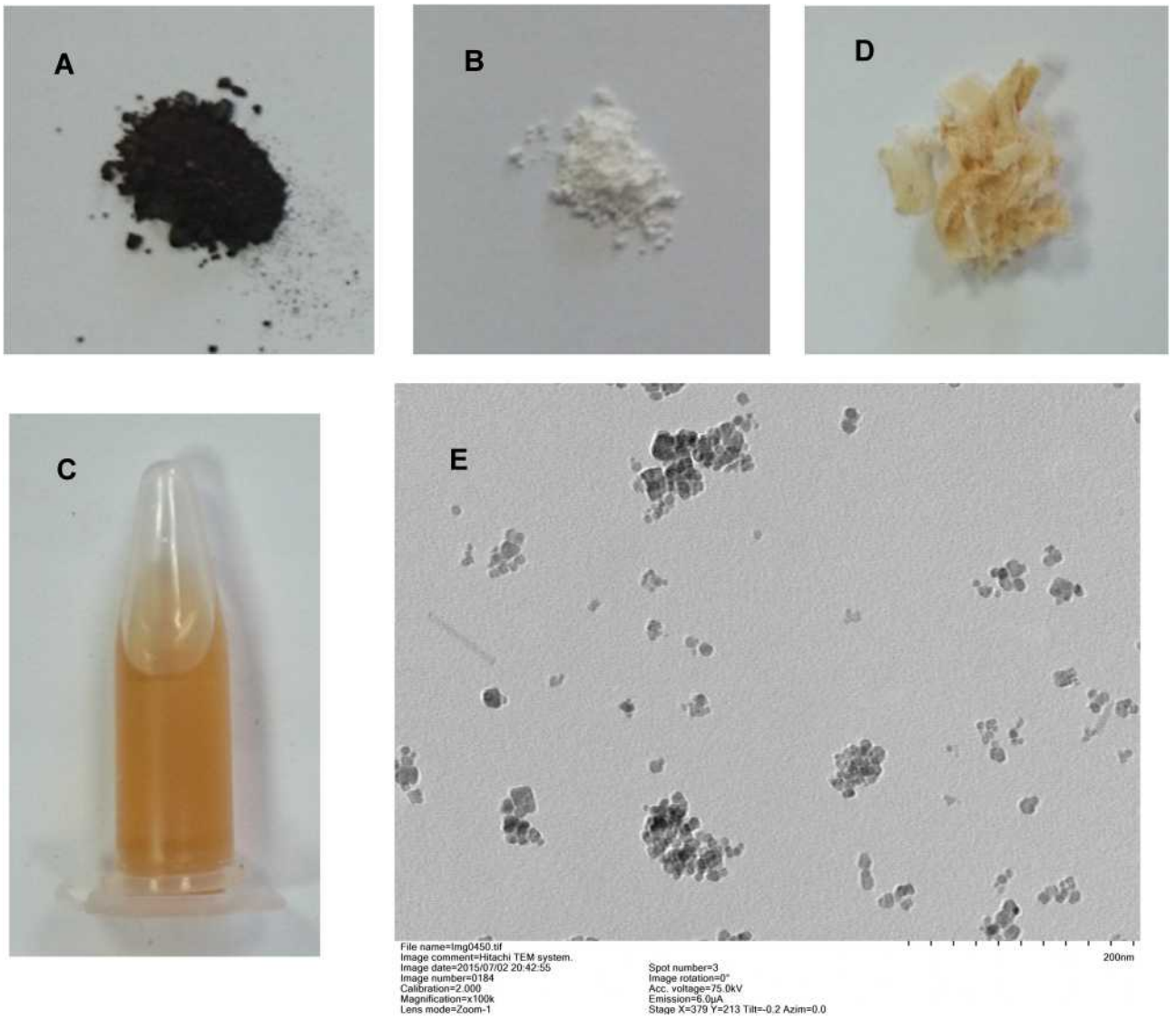

Figure 1 Oleic acid-coated IONPs (**A**) modified with cobalt-60 irradiated LMWHA (**B**) to form an LMWHA-IONP solution (**C**). Freeze-drying was carried out to obtain powdered LMWHA-IONPs (**D**). Transmission electron microscopy (TEM) image of prepared LMWHA-IONPs shows excellent dispersive property. Particles exhibited a spherical core and were surrounded by a transparent oil shell (**E**).

paraformaldehyde. Cell membranes were punctured with 0.1% Triton x-100 and 4.6-diamidino-2-phenylindole (DAPI) was added to each cover glass to enhance nuclear staining. After staining, the cover glasses were mounted on cover slides with Prolong® Diamond Antifade Mountant (Molecular Probes™, Life Technologies, Monza, Italy), and fluorescence images were obtained using a fluorescence microscope (Leica DMi8, Leica Microsystems, Wetzlar, Germany) fitted with a CCD camera (Leica DFC7000 T).

Cytotoxicity of LMWHA-Fe_3O_4 NPs

The cytotoxicity of LMWHA and LMWHA-IONPs was tested on NIH3T3 and U87MG cells using the standard ISO 10993-5 procedure. Prior to the test, 400 mg of LMWHA-IONPs were immersed in 2 mL DMEM at 37°C for 24 hours. The supernatant was then added to cultured NIH3T3 and U87MG cells until reaching a concentration of 0.2 mg/mL. For each cell line, cytotoxicity was determined using the MTT (3-(4,5-Dimethylthiazol-2-yl)-2,5-diphenyltetrazolium bromide) method by reading the 570/690 nm absorbance using a microplate reader (EZ Read 400, Biochrom, Holliston, MA, USA). During these tests, DMEM containing 2% dimethyl sulfoxide (DMSO) was used as the positive control, while cells cultured without additive were used as a blank group.

Time-of-Flight Secondary Ion Mass Spectrometry Analysis

NIH3T3 and U87MG cells were cultured in 6-well culture plates at a density of 5×10^5 cells/mL for 24 hours. 1 mg/mL of LMWHA-IONPs was then added to the culture media for an additional 24 hours. The media were removed and cells washed twice with PBS and then fixed with glutaraldehyde. Time-of-flight secondary ion mass spectrometry (TOF-SIMS) (PHI TRIFT IV, ULVAC-PHI, Kanagawa, Japan) was performed by applying a Bi_3^+ primary ion beam (operated at 30 keV) to the sample surface.[44] The binding of LMWHA-IONPs to NIH3T3 and U87MG cell surfaces was evaluated by detecting the Fe ion signal (m/z 56) and phospholipid (m/z 86 and m/z 184) signals[45,46] over a surface area of 200×200 μm^2.

Fe Ion Content on Cell Surface

The targeting ability of LMWHA-IONPs was determined by evaluating the quantity of Fe ions on cell surfaces using the thiocyanate method. NIH3T3 and U87MG cells with various densities ($1.0\times10^4 \sim 5.0\times10^5$ cells/mL) were pre-treated with 1 mg/mL LMWHA-IONPs for 24 hours. 30% hydrochloric acid was added to the cells and the resulting solution maintained at 55 °C for 3 hours. Ammonium persulfate was added and the solution was left to stand at room temperature for 15 minutes. Finally, the formed Fe^{3+} ions were reacted with SCN^- ions by adding potassium thiocyanate (KSCN) to the solution. The resulting blood-red complex $[Fe(SCN)_6]^{3-}$ was detected by a microplate reader (EZ Read 400, Biochrom, Holliston, MA, USA) at a wavelength of 570 nm. Finally, the concentration of IONPs on the cell surfaces was determined by referencing a calibration curve constructed using the optical density readings obtained for a series of standard solutions with known Fe^{3+} concentrations.

T2*-Weighted Images of Cells Treated with LMWHA-Fe_3O_4 NPs

NIH3T3 and U87MG cells were cultured with 2 mg/mL of LMWHA-IONPs for 24 hours in culture medium at room temperature. Phantom samples for MRI imaging were prepared according to a previous report.[47] Briefly, 5 mL agarose gel was filled into each well of a 6-well culture plate and placed in an ultrasound bath to remove air bubbles. Meanwhile, labeled NIH3T3 and U87MG cells were washed twice with PBS and then re-suspended in PBS. Cell suspensions with concentrations of 1.0×10^5, 5.0×10^5 and 1.0×10^6 cells/mL were mixed with agarose and filled into the wells containing agarose described above. Following ultrasound treatment, the plate was allowed to cool and an additional 5 mL of agarose was added to cover the resulting cell layer. MRI imaging was then performed using a 1.5 T MRI device (Signa HDxt superconductor clinical MR system, GE Medical Systems, Milwaukee, WI, USA). For each cell line, the phantom dish was placed in the magnetic field chamber of the MRI device and T2* weighted images were acquired with a slice thickness of 4 mm, a repetition time of 170 msec, an echo time of 6.756 msec, an echo number of 1, an echo train length of 1, a matrix size of 256 × 256, a pixel bandwidth of 114.922, a flip angle of 20°, and a specific absorption rate of 0.00354923. Quantification of the labeled cells in the gel samples was performed by measuring the gray level of the detected T2* weighted images using commercial image analysis software (Image Pro Plus, Media Cybernetics, Inc., Silver Spring, MD, USA).

Statistical Analysis

For fluorescence intensity, cell viability, and Fe ion content tests, the mean values and standard deviations of each measurement were recorded. One-way analysis of variance (ANOVA) with Tukey's post hoc tests (SPSS Inc., Chicago, IL, USA) were performed to examine differences between samples. A *p*-value lower than 0.05 was considered to be statistically significant in each case.

Results

Morphology of the oleic-acid coated IONPs was observed by TEM (Figure 1E). These particles exhibited a spherical core surrounded by a transparent oil shell. The OA-IONPs demonstrated a good dispersibility in water (Figure 1E) with a polydispersity index (PDI) of 0.132. OA-IONP diameters were found to be concentrated in the range of 4~12 nm (94.4%) with a average of 6.13 nm (Figure 2A). The Zeta potential read from the electrophoretic light scattering device was −48.22 mV. When NPs were conjugated with the γ-ray irradiated LMWHA, particle diameter increased to 500~900 nm (72.1%) (Figure 2B).

When NIH3T3 cells were treated with FITC-labeled LMWHA (control group), only the nuclei showed a blue color (Figure 3A and B). However, when U87MG cells were treated with FITC-labeled LMWHA, obvious green fluorescent signals were observed (Figure 3C and D) on cell

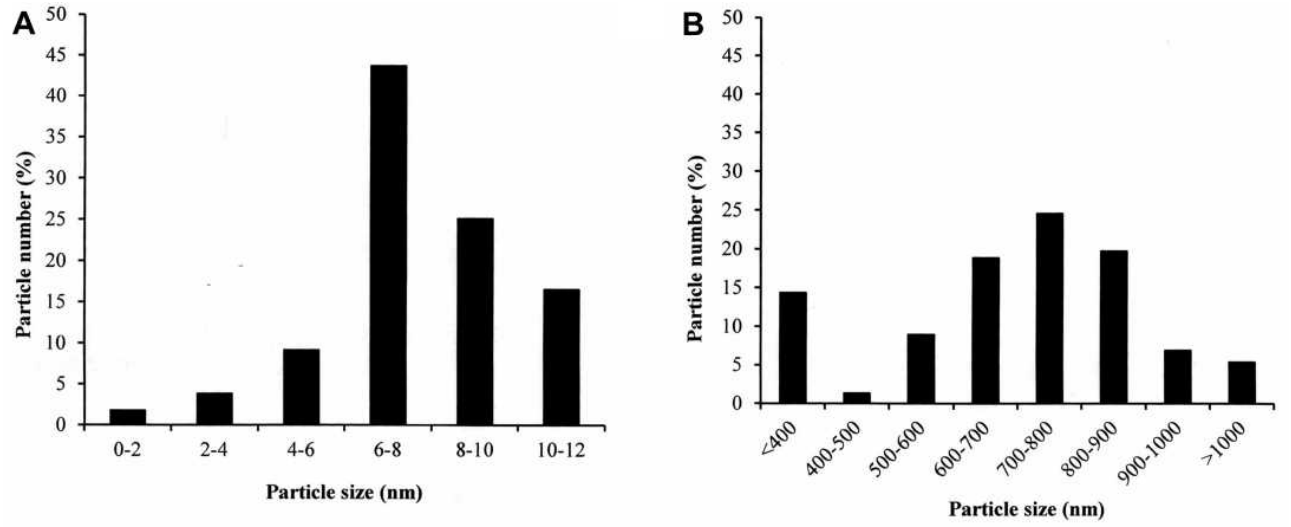

Figure 2 Particle diameter distributions of (**A**) oleic acid-coated IONPs and (**B**) LMWHA-IONPs.

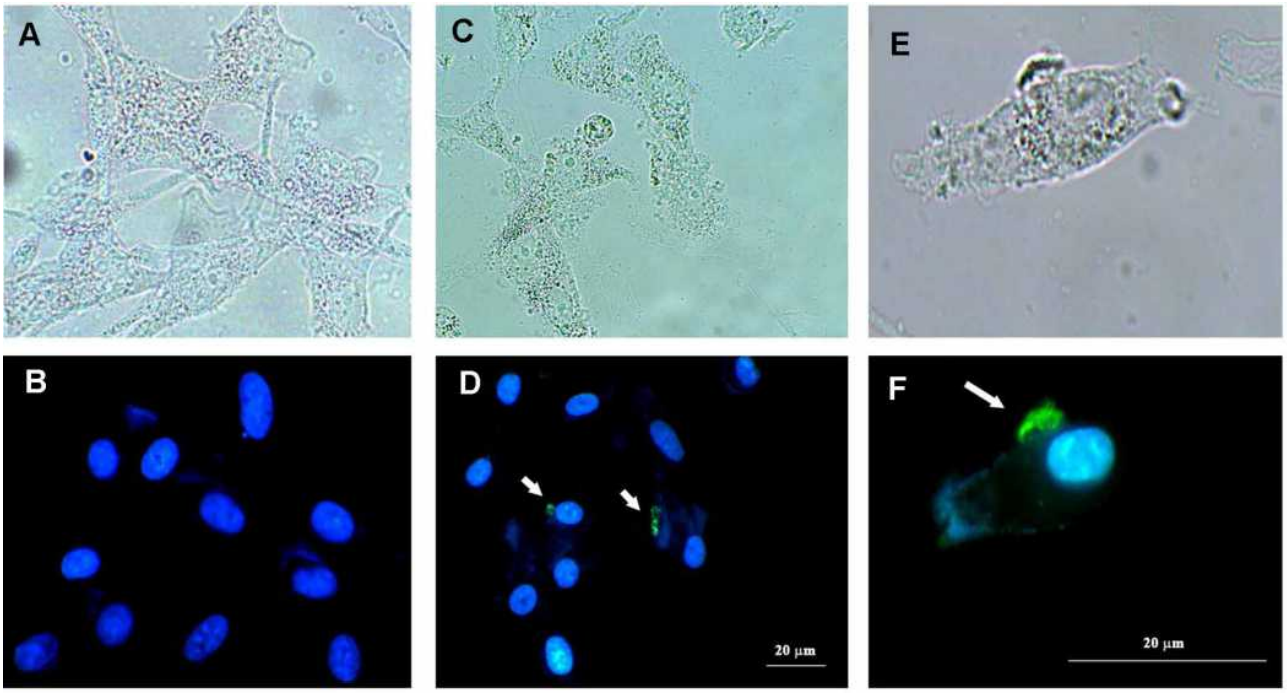

Figure 3 Optical (**A, C, E**) and fluorescent (**B, D** and **F**) microscope images of NIH3T3 (**A** and **B**) and U87MG (c, d) cells co-cultured with FITC-labeled LMWHA. FITC-labeled LMWHA (green fluorescence) is observed on surface of U87 MG cells (**F**). White arrows identify FITC-labeled LMWHA on the cell surface.

surfaces (Figure 3E and F). Figure 4 shows detected fluorescence intensities of the NIH3T3 and U87MG cells seeded at various densities and cultured with different concentrations of FITC-labeled LMWHA. For both cells lines, fluorescence intensity increased with increasing cell density and culture concentration. However, for each cell density and LMWHA concentration, U87MG cells exhibited higher fluorescence intensity than NIH3T3 cells. For example, the NIH3T3 cells had a maximum fluorescence intensity of 1257.3 ± 103.3 when seeded with a density of 5×10^4 cells/mL and cultured with 4 mg/mL FITC-labeled LMWHA (Figure 4A), whereas U87MG cells exhibited a fluorescence intensity of 9896.7 ± 400.5 (an improvement of almost 8 times) under the same culturing conditions (Figure 4B).

Viability of NIH3T3 and U87MG cells was evaluated using MTT assays. Cells cultured with DMSO showed

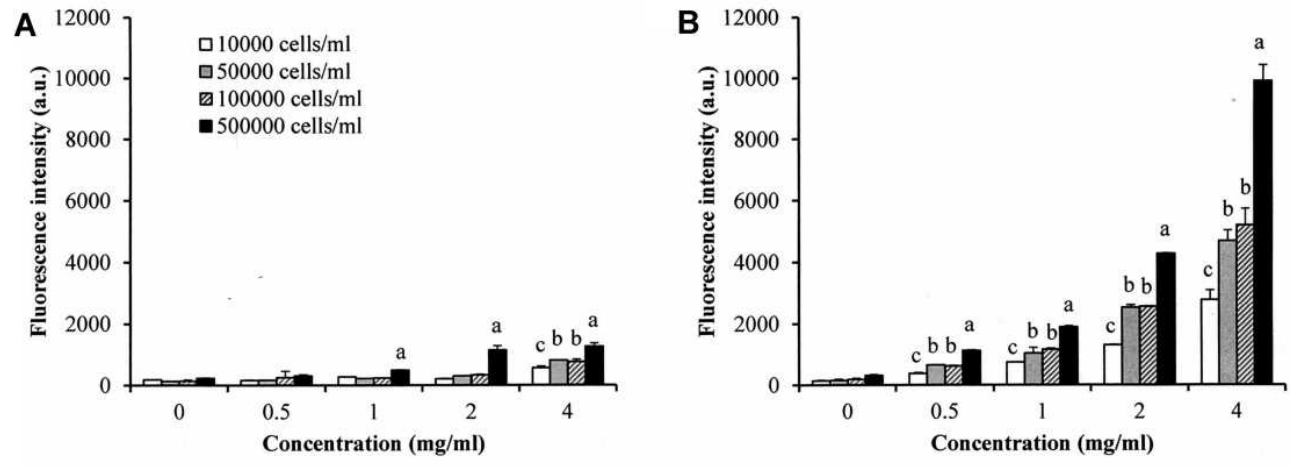

Figure 4 Quantitative analysis of fluorescence intensities of (**A**) NIH3T3 and (**B**) U87MG cells co-cultured with FITC-labeled LMWHA. (Values not sharing the same letter are significantly different ($p < 0.01$).).

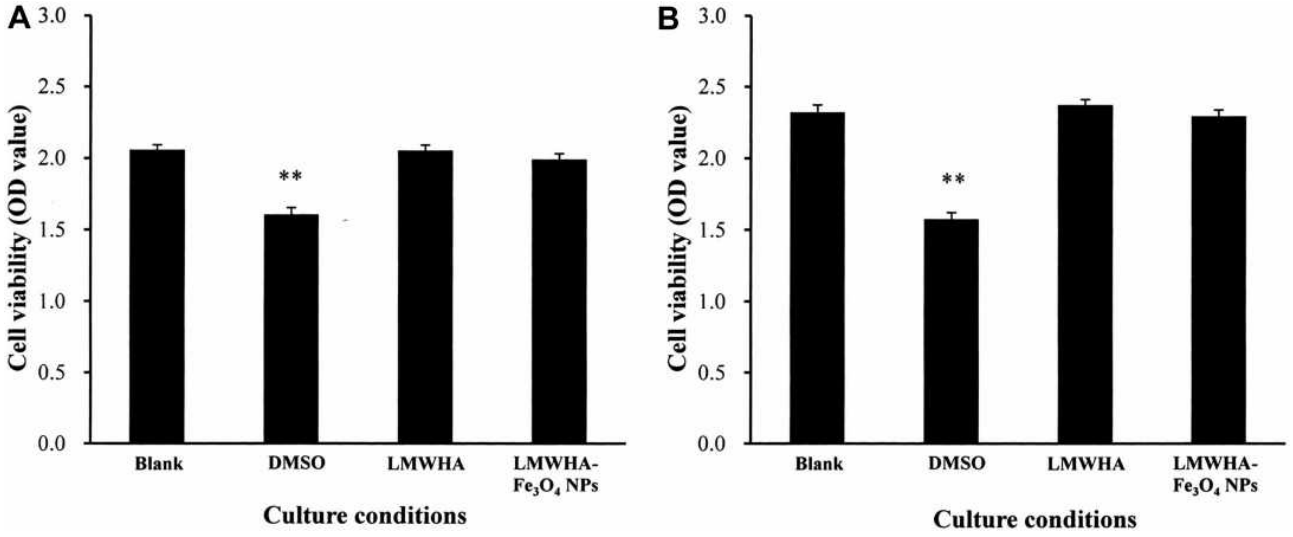

Figure 5 Cell proliferation assay results for (**A**) NIH3T3 and (**B**) U87MG cells cultured with neat LMWHA and LMWHA-IONPs. **Denotes $p < 0.01$.

a significantly lower viability than the blank sample (Figure 5). However, no significant change was observed in the viabilities of cells treated using LMWHA or LMWHA-IONPs.

Figure 6 shows the TOF-SIMS images of the NIH3T3 (upper) and U87MG (lower) cells co-cultured with LMWHA-IONPs. Note that the m/z 56, 86 and 186 signals correspond to Fe ions, $C_5H_{12}N^+$ fragments, and the head group ($C_5H_{15}NPO_4^+$) of phosphatidylcholine on the cellular membrane, respectively. Comparing the m/z 56 signals of the two cell lines, it is seen that the U87MG group signal is more pronounced and abundant than that of the NIH3T3 group. Figure 7 shows the m/z 56 and 186 convolution images of the two cells. For U87MG cells (Figure 7B), the m/z 56 signal is located mainly around the boundary of m/z 186 (the $C_5H_{12}N^+$ fragments). In other words, the IONPs mainly target the cellular surface rather than the cell interior.

The quantity of Fe ions on NIH3T3 and U87MG cells cultured with LMWHA-IONPs was determined using the thiocyanate colorimetry method. Fe ion content on U87MG cells was significantly higher than on NIH3T3 cells for each of the considered culture concentrations (Figure 8). For example, given a seeding density of 1.0×10^4 cells/mL, the quantity of Fe ions on U87MG cells was 1.4 times higher than on NIH3T3 cells ($p < 0.01$). Moreover, at the highest seeding density of 5.0×10^5 cells/mL, the difference between Fe ion contents of the two cell lines increased to almost three times ($p < 0.01$).

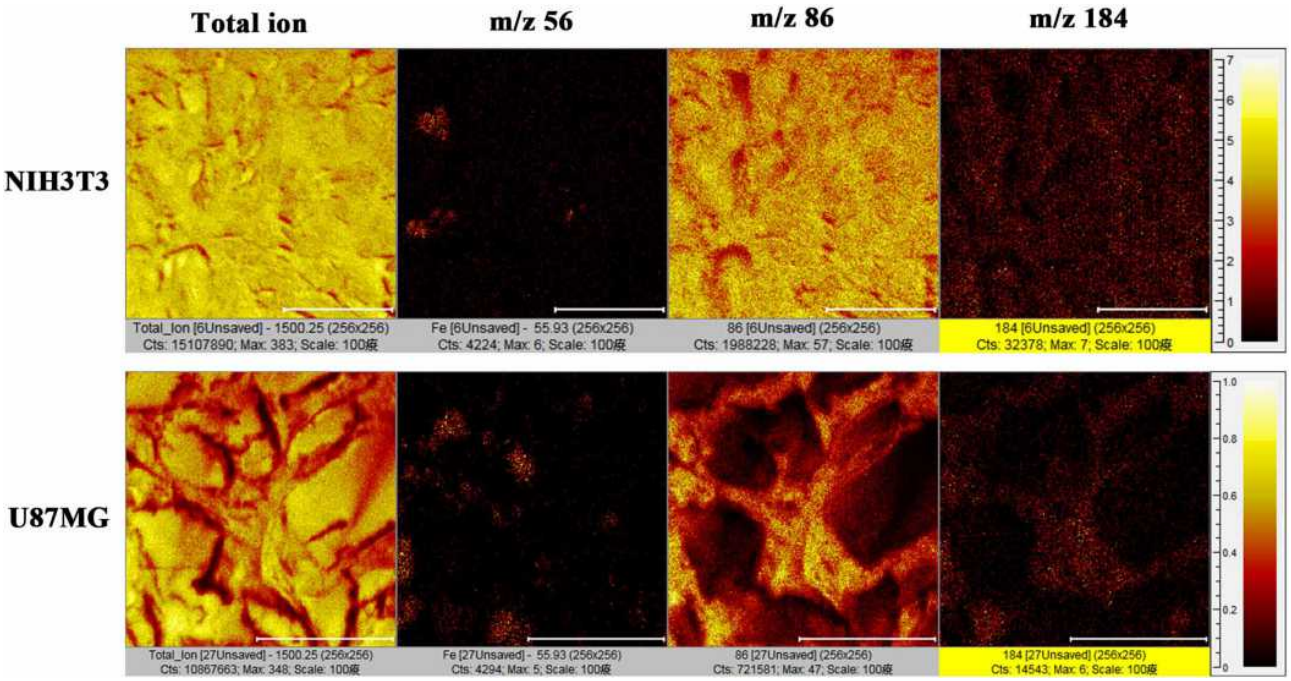

Figure 6 TOF-SIMS images of NIH3T3 and U87MG cells co-cultured with LMWHA-IONPs. (Note that m/z 56, 86 and 186 signals represent Fe ions, $C5H12N^+$ fragments, and head group ($C5H15NPO4^+$) of PC on cellular membrane, respectively. Scale bar indicates 100 μm.).

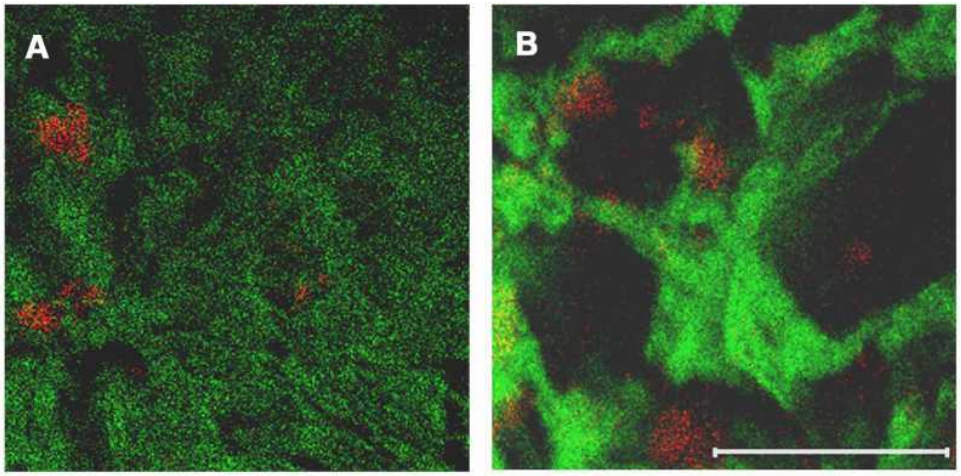

Figure 7 Convolution TOF-SIMS images of (**A**) NIH3T3 and (**B**) U87MG cells cultured with LMWHA-IONPs. The m/z 56 signal (red image representing Fe ions) in Fig. (**B**) shows enhanced targeting of LMWHA-IONPs on U87MG cellular surface. (Scale bar indicates 100 μm.).

T2* weighted MR images of IONPs showed a black pattern (Figure 9A) compared to the blank control (Figure 9B). Images for NIH 3T3 (Figure 9C) and U87MG (Figure 9D) cells cultured without LMWHA-IONPs were clear and white. The T2* weighted MR images of the tested NIH 3T3 and U87MG cells were captured (Figure 10A) and the signal intensity quantified. For both cell lines, the intensity of T2* weighted MR images reduced with an increasing cell density (Figure 10B). However, at a cell density of 1.0×10^5 cells/mL, the signal intensity of U87MG cells was around 1.1 times higher than that of NIH3T3 cells. Furthermore, at the highest cell density of 1.0×10^6 cells/mL, the signal intensity of U87MG cells increased to around 1.3 times that of NIH3T3 cells ($p < 0.05$).

Discussion

It has been reported that several biodegradable and biocompatible materials such as poly-l-lysine, citric acid, oleic acid, and carboxymethyl-dextran can be used as coating agents for obtaining stabilized and biocompatible

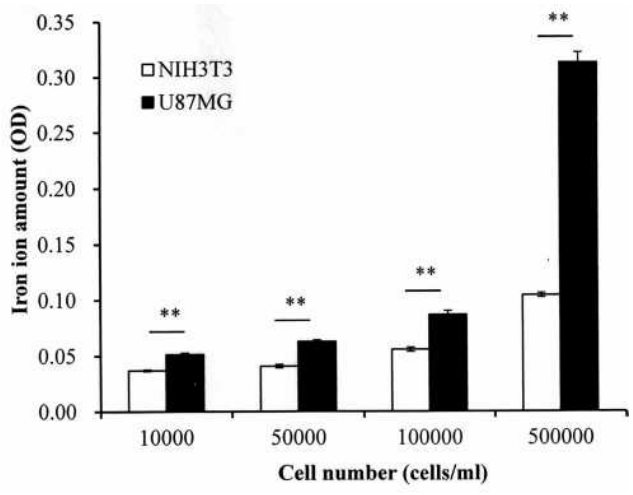

Figure 8 Quantitative analysis of Fe ions on surfaces of NIH3T3 and U87MG cells with different seeding densities. **Denotes $p < 0.01$.

IONPs.[9,14,15,48] In this study, the surfaces of IONPS were coated with OA during the NP preparation process in order to minimize the oxidation effect and reduce particle agglomeration. In 2020, Tiar and coauthors tested IONPs coated with various fatty acids and found that IONPs coated with OA exhibited the smallest PDI (0.154), hydrodynamic size, and a narrow particle size distribution when compared to IONPs coated with other fatty acids.[49] In this study, The PDI of prepared OA-IONPs (0.132) was close to the result of the previous study, and the zeta potential of the prepared OA-IONPs was found to vary in the range of −40 mV to −60 mV. Collectively, these physical characteristics and the TEM image presented in Figure 1E, provide proof that the prepared OA-coated IONPs have good dispersibility.[15,42] In addition, the majority of these

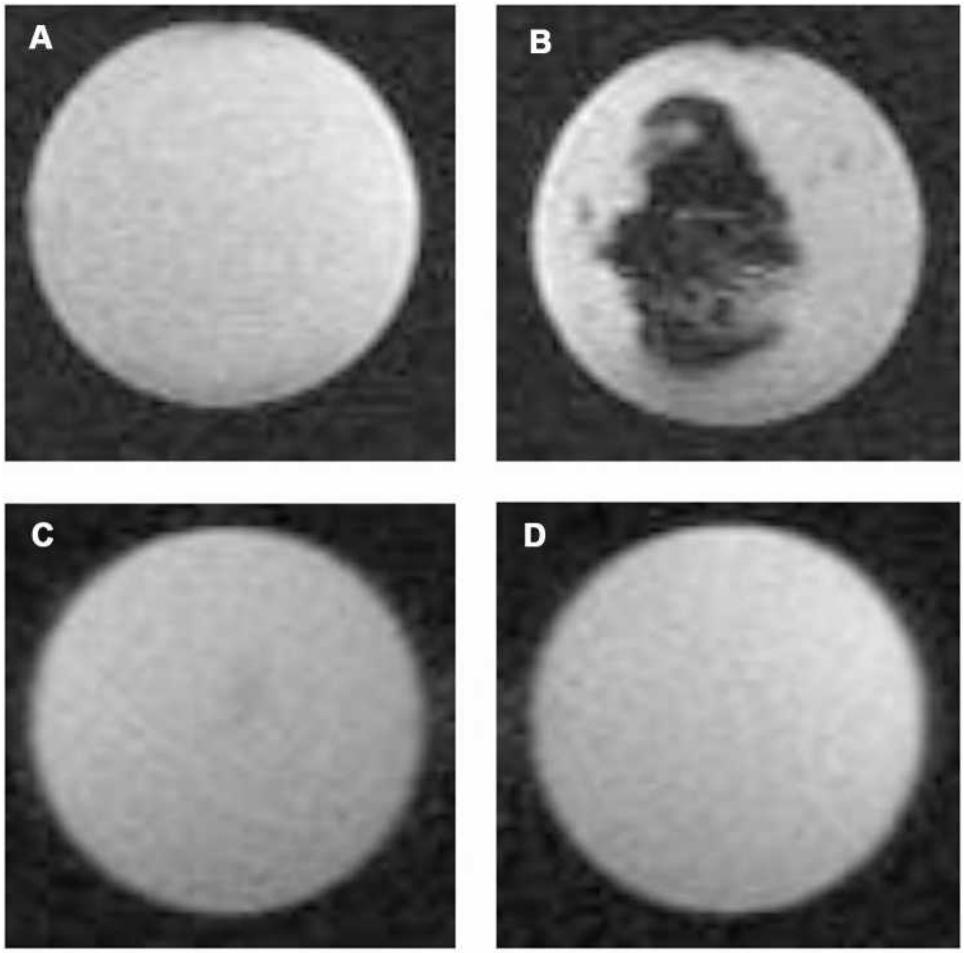

Figure 9 T2* weighted images of the (**A**) blank, and (**B**) LMWHA-IONPs in agarose. (**C**) and (**D**) show T2* weighted images of agarose with NIH3T3 and U87MG cells cultured under LMWHA-IONPs free conditions.

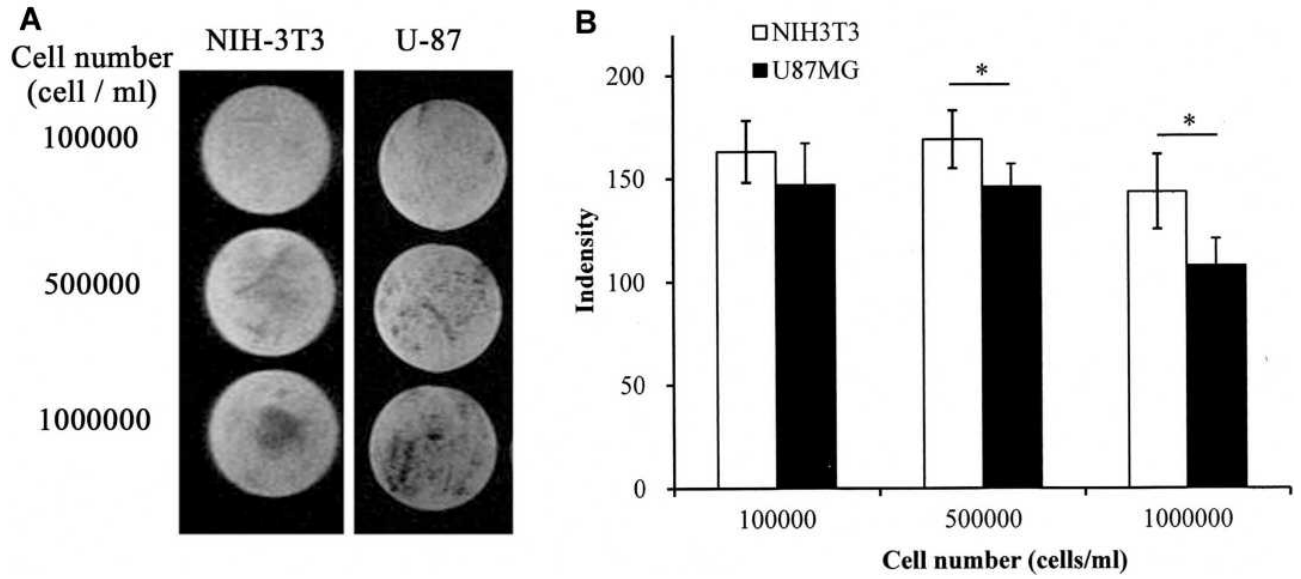

Figure 10 (**A**) T2* weighted images of NIH3T3 and U87MG cells cultured with LMWHA-IONPs at different seeding densities. (**B**) Quantitative analysis of T2* weighted images. *Denotes $p < 0.05$.

prepared IONPs have a diameter ranging from 4 to 12 nm (Figure 2A). This diameter is less than 30 nm; hence, it can be inferred that these IONPs are superparamagnetic.[10] Notably, even though the LMWHA-IONPs have a much larger diameter of 500–1000 nm, this has no apparent effect on their properties as an MRI imaging material.[42] In actuality, the major effect of particle size of IONP on MRI imaging is to determine suitability for application as a negative or positive contrast agent.[3] It has been reported that a large nanoparticle size can enhance negative contrast while a small analog can enhance the positive contrast of MR images.[3] Because the HA used in this study did not involve the imaging process, it is reasonable to suggest that the IONPs fabricated in this study are adequate for the fabrication of MRI contrast agent.

Nanoscale fluorescent probes have been developed that improve the operation of cancer treatments, such as magnetic hyperthermia.[50] Qhattal and Liu (2011) investigated the effect of HA molecular weight on endocytosis of HA-grafted liposomes by cancer cells.[28] Their results showed that the cellular targeting efficiency of HA depends strongly upon molecular weight. Since the specific ability of fluorescence-labeled HA to target cancer cells has been reported in previous studies, this was used as the control group in the present study.[51] Figure 3B and D present fluorescence images of the present NIH3T3 and U87MG cells co-cultured with FITC-labeled LMWHA. The U87MG cells exhibited a greater number of surface fluorescence spots (Figure 3F). In other words, the γ-irradiated LMWHA successfully targets the HA receptors on the U87MG cell surface. Referring to Figure 4, it can be seen that for a given cell density and culture concentration, fluorescence intensity of U87MG cells (Figure 4B) is around 8 times higher than that of NIH3T3 cells (Figure 4A). This finding is reasonable since U87MG is a cancer cell, and therefore contains a greater number of CD44 receptors on its cell membrane compared to normal fibroblasts.[26,27] Notably, since the ability of γ-irradiated LMWHA to target tumor cells is different for normal cells, γ-irradiated LMWHA has significant potential as a modifier for producing MRI contrast agents.

Biocompatibility is a crucial concern for the clinical application of MRI contrast agents. For example, a high dose of Mg-based MRI contrast agent may have serious adverse effects on some patients.[6,7] Hence, HA is commonly used to modify the surface of MRI contrast agents in some way to reduce their cytotoxicity and improve their stability.[8] Fe_3O_4 NPs are a common candidate for the production of MRI contrast agents. However, while polymer-coated Fe_3O_4 NPs have an excellent contrast performance,[13] their toxicity poses a serious concern in biomedical applications.[52] Consequently, many studies have employed HA to conjugate magnetic NPs with improved biocompatibility and reduced cytotoxicity.[8,29,30] In the present study, cytotoxicity of fabricated IONP composites were assayed on NIH3T3 fibroblasts and U87MG

glioblastoma cells according to the ISO 10993–5 standard, as was done in a previous study.[15] Our results showed that U87MG and NIH3T3 cells treated with neat LMWHA or LMWHA-IONPs showed no significant difference in viability compared to the blank group (Figure 5). In other words, the present results are consistent with previous studies that showed treatment with γ-irradiated HMWHA has no effect on the vitality of biological cells.[15,29,30]

Mass spectrometry imaging (MSI) is an important analytical tool for label-free chemical imaging of diverse molecules in biological specimens.[53] Secondary ion and laser desorption ionization MS are two major MSI devices used for simultaneous detection of NPs and biomolecules.[54] There is potential use of MSI image data as a base for future big data and machine learning imaging applications.[55,56] TOF-SIMs is a highly sensitive cell surface analysis technology in which a high-energy primary ion beam (a Bi^{3+} ion beam in the present study) is used to ionize the surface of a tested sample so that the secondary ionized molecular fragments emitted from the sample surface can be analyzed. By examining the m/z signals of these secondary ions, both the entire image of the whole tissue and that of specific chemical fragments can be reconstructed.[45,57] In performing the TOF-SIMS analysis of cellular membranes, Nygren et al chose phosphatidylcholine (PC), an abundant phospholipid on the cellular membrane, as a detecting target and used m/z 86 ($C_5H_{12}N^+$ fragments) and m/z 184 (head group ($C_5H_{15}NPO_4^+$) of PC) signals to reconstruct the image.[45,46,57] TOF-SIMs images have been widely used for analyzing the interaction between inorganic materials and cells. For example, Kokesch-Himmelreich et al cultured osteoblast-like cells on strontium-enriched bone cement and analyzed their mineralized extracellular matrix by TOF-SIMs. Their results confirmed that metal ions released by artificial biomaterials and subsequently accumulated within biological cells can be detected by TOF-SIMs.[45]

In the present study, TOF-SIMs images of NIH3T3 and U87MG cells co-cultured with LMWHA-modified IONPs showed that U87MG cells exhibited an obviously stronger Fe ion signal (m/z 56) than NIH3T3 cells (Figure 7). This result is consistent with the finding that γ-ray irradiated LMWHA has a strong ability to target the surface of U87MG glioblastoma cells (Figure 3). In addition, Figure 8 shows that U87MG cells have a far higher Fe ion content than NIH3T3 cells. Thus, combining these results with those shown for fluorescence intensity (Figure 4), it can be confirmed that LMWHA-IONPs provide an effective means of distinguishing tumor cells from normal cells.

To investigate NPs modified by HA for cancer imaging, Payne et al compared the contrast in MR and fluorescence imaging.[51] Their results demonstrated that HA incorporating magnetic NPs and a fluorophore provides a significant contrast enhancement effect for tumor resections and is thus beneficial in improving the patient's prognosis. In the present study, the ability of LMWHA-IONPs to target CD44-abundant glioblastoma cells was investigated by both fluorescence observations (Figure 3) and MR imaging (Figure 10). Imaging results showed that as cell density increased, the intensity of the MR image reduced significantly for both U87MG and NIH3T3 cell lines. In other words, the contrast of the corresponding T2* weighted images was improved in both cases. It is noted that these findings are consistent with those of previous reports on the use of HMWHA-IONPs as a MR contrast agent.[36,41,42] A quantitative analysis showed that the reduction in the image intensity for U87MG glioblastoma cells was higher than for NIH3T3 cells (Figure 10B). This result is to be expected since there are more CD44 receptors on the cellular membrane of cancer cells (glioblastoma) than on normal fibroblast cells,[8,26,27] and hence LMWHA-IONPs show a stronger targeting ability.

It has been reported that IONPs can also be used in various antitumor treatments. For example, during magnetic hyperthermia and photothermal therapy, alternating magnetic fields and near-infrared lasers can trigger IONPs in the tumor cells and heat the tumor by typically 41–55 °C, which results in the destruction of tumor cells. In addition, photo-dynamic therapy can trigger IONPs in tumor cells and induce antitumor activity through the release of radical oxygen species.[15,58] However, in order to achieve this antitumor goal, two points must be met: First, IONPS need to be internalized by tumor cells.[16,59] In 2019, Alphandery et al tested the antitumor activity of IONPs synthesized from magnetotactic bacteria (magnetosomes). They found that these chained IONPs can be internalized in U87MG cells so that tumor cells can be destroyed by exposure to an alternating magnetic field.[59] Second, the amount of IONP must be sufficient, reaching a concentration of 1 mg/mL.[16,60,61] However, as seen in Figures 3 and 7, the probe-conjugated LWMHA can target only cell surfaces and not the inside of U87MG cells. This may be due to the HA modification increasing the overall particles volume and preventing the LMWHA-modified INOPs from entering and accumulating inside the cells.

This is a possible limitation for the application of current LMWHA-modified INOPs in an anti-glioblastoma role.

Conclusion

In conclusion, the LMWHA-IONPs prepared in the present study have shown a strong specific-binding ability to U87MG glioblastoma cells. As a result, they yield a significant improvement in the MR image contrast of cancer cells. Hence, even though further in vivo and animal experiments are required, it appears that LMWHA-IONPs have significant potential as an MRI contrast agent for the detection of cancer and tumor cells.

Abbreviations

FITC, Fluorescein-5-isothiocyanate; HA, Hyaluronic acid; HMWHA, high-molecular-weight hyaluronic acid; IONPs, iron oxide nanoparticles; KSCN, potassium thiocyanate, LMWHA, low-molecular-weight hyaluronic acid; DLS: dynamic light scattering; MRI, magnetic resonance imaging; OA, oleic acid; TEM, transmission electron microscope; TOF-SIMS, time-of-flight secondary ion mass spectrometry; MSI, mass spectrometry imaging; PDI: polydispersity index.

Acknowledgments

This work was performed with the support from the Core Facility Center, Office of Research and Development, Taipei Medical University, Taipei, Taiwan.

Disclosure

The authors report no conflicts of interest in this work.

References

1. Major JL, Meade TJ. Bioresponsive, cell-penetrating, and multimeric MR contrast agents. *Acc Chem Res*. 2009;42(7):893–903. doi:10.1021/ar800245h
2. Yan GP, Robinson L, Hogg P. Magnetic resonance imaging contrast agents: overview and perspectives. *Radiography*. 2007;13:5–19. doi:10.1016/j.radi.2006.07.005
3. Alphandéry E. Iron oxide nanoparticles as multimodal imaging tools. *RCS Adv*. 2019;9:40577–40578.
4. Geng WX, Zheng Z, Guo DS. Supramolecular design based activatable magnetic resonance imaging. *VIEW*. 2020;2(2):20200059. doi:10.1002/VIW.20200059
5. Katti G, Ara SA, Shireen A. Magnetic resonance imaging (MRI)-A review. *Int J Clin Dent*. 2011;3:65–70.
6. Sieber MA, Steger-Hartmann T, Lengsfeld P, Pietsch H. Gadolinium-based contrast agents and NSF: evidence from animal experience. *J Magn Reson Imaging*. 2009;30(6):1268–1276. doi:10.1002/jmri.21971
7. Fu C, Duan X, Cao M, et al. Targeted magnetic resonance imaging and modulation of hypoxia with multifunctional hyaluronic Acid-MnO2 nanoparticles in glioma. *Adv Healthc Mater*. 2019;8(10):e1900047. doi:10.1002/adhm.201900047
8. Lee T, Lim EK, Lee J, et al. Efficient CD44-targeted magnetic resonance imaging (MRI) of breast cancer cells using hyaluronic acid (HA)-modified MnFe2O4 nanocrystals. *Nanoscale Res Lett*. 2013;8(1):149. doi:10.1186/1556-276X-8-149
9. Alphandéry E. Applications of magnetotactic bacteria and magnetosome for cancer treatment: a review emphasizing on practical and mechanistic aspects. *Drug Discov Today*. 2020;25(8):1444–1452. doi:10.1016/j.drudis.2020.06.010
10. Shen YF, Tang J, Nie ZH, Wang YD, Ren Y, Zuo L. Preparation and application of magnetic Fe3O4 nanoparticles for wastewater purification. *Sep Purif Technol*. 2009;68(3):312–319. doi:10.1016/j.seppur.2009.05.020
11. Lee N, Hyeon T. Designed synthesis of uniformly sized iron oxide nanoparticles for efficient magnetic resonance imaging contrast agents. *Chem Soc Rev*. 2012;41(7):2575–2589. doi:10.1039/C1CS15248C
12. Gallo J, Kamaly N, Lavdas I, et al. CXCR4-targeted and MMP-responsive iron oxide nanoparticles for enhanced magnetic resonance imaging. *Angew Chem Int*. 2014;53(36):9550–9554. doi:10.1002/anie.201405442
13. Karimzadeh I, Aghazadeh M, Doroudi T, Ganjali MR, Kolivand PH. Superparamagnetic iron oxide (fe_3o_4) nanoparticles coated with peg/pei for biomedical applications: a facile and scalable preparation route based on the cathodic electrochemical deposition method. *Adv Phys Chem*. 2017;9437487.
14. Alphandéry E. Iron oxide nanoparticles for therapeutic applications. *Drug Discov Today*. 2020;25(1):141–149. doi:10.1016/j.drudis.2019.09.020
15. Mandawala C, Chebbi I, Durand-Dubief M, et al. Biocompatible and stable magnetosome minerals coated with poly-l-lysine, citric acid, oleic acid, and carboxy-methyl-dextran for application in the magnetic hyperthermia treatment of tumors. *J Mater Chem B*. 2017;5(36):7644–7660. doi:10.1039/C6TB03248F
16. Curcio A, Silva AKA, Cabana S, et al. Iron oxide nanoflowers @ CuS hybrids for cancer tri-therapy: interplay of photothermal therapy, magnetic hyperthermia and photodynamic therapy. *Theranostics*. 2019;9(5):1288–1302. doi:10.7150/thno.30238
17. Liang C, Zhang X, Cheng Z, Yang M, Huang W, Dong X. Magnetic iron oxide nanomaterials: a key player in cancer nanomedicine. *VIEW*. 2020;1(3):20200046. doi:10.1002/VIW.20200046
18. Alphandéry E. Biosynthesized iron oxide nanoparticles for cancer treatment. *Int J Pharm*. 2020;586:119472. doi:10.1016/j.ijpharm.2020.119472
19. Gupta AK, Gupta M. Synthesis and surface engineering of iron oxide nanoparticles for biomedical applications. *Biomaterials*. 2005;26(18):3995–4021. doi:10.1016/j.biomaterials.2004.10.012
20. Korn P, Schulz MC, Hintze V, et al. Chondroitin sulfate and sulfated hyaluronan-containing collagen coatings of titanium implants influence peri-implant bone formation in a minipig model. *J Biomed Mater Res A*. 2014;102(7):2334–2344. doi:10.1002/jbm.a.34913
21. Vigetti D, Karousou E, Viola M, Deleonibus S, De Luca G, Passi A. Hyaluronan: biosynthesis and signaling. *Biochim Biophys Acta Gen Subj*. 2014;1840(8):2452–2459. doi:10.1016/j.bbagen.2014.02.001
22. Frenkel JS. The role of hyaluronan in wound healing. *Int Wound J*. 2014;11(2):159–163. doi:10.1111/j.1742-481X.2012.01057.x
23. Ganau M, Syrmos NC, D'Arco F, et al. Enhancing contrast agents and radiotracers performance through hyaluronic acid-coating in neuroradiology and nuclear medicine. *Hell J Nucl Med*. 2017;20(2):166–168. doi:10.1967/s002449910558
24. Rutjes AW, Jüni P, Costa BRD, Trelle S, Nüesch E, Reichenbach S. Viscosupplementation for osteoarthritis of the knee: a systematic review and meta-analysis. *Ann Intern Med*. 2012;157(3):180–191. doi:10.7326/0003-4819-157-3-201208070-00473
25. Zhang R, Rejeeth C, Xu W, et al. Label-free electrochemical sensor for CD44 by ligand-protein interaction. *Anal Chem*. 2019;91(11):7078–7085. doi:10.1021/acs.analchem.8b05966

26. Toole BP. Hyaluronan-CD44 interactions in cancer: paradoxes and possibilities. *Clin Cancer Res*. 2009;15(24):7462–7468. doi:10.1158/1078-0432.CCR-09-0479
27. Kim K, Choi ES, Choi ES, Park MH, Ryu JH. Hyaluronic acid-coated nanomedicine for targeted cancer therapy. *Pharmaceutics*. 2019;11(7):301. doi:10.3390/pharmaceutics11070301
28. Qhattal HS, Liu X. Characterization of CD44-mediated cancer cell uptake and intracellular distribution of hyaluronan-grafted liposomes. *Mol Pharm*. 2011;8(4):1233–1246. doi:10.1021/mp2000428
29. Kamat M, El-Boubbou K, Zhu DC, et al. Hyaluronic acid immobilized magnetic nanoparticles for active targeting and imaging of macrophages. *Bioconjug Chem*. 2010;21(11):2128–2135. doi:10.1021/bc100354m
30. Li J, He Y, Sun W, et al. Hyaluronic acid-modified hydrothermally synthesized iron oxide nanoparticles for targeted tumor MR imaging. *Biomaterials*. 2014;35(11):3666–3677. doi:10.1016/j.biomaterials.2014.01.011
31. Aya KL, Stern R. Hyaluronan in wound healing: rediscovering a major player. *Wound Repair Regen*. 2014;22(5):579–593. doi:10.1111/wrr.12214
32. Cyphert JM, Trempus CS, Garantziotis S. Size matters: molecular weight specificity of hyaluronan effects in cell biology. *Int J Cell Biol*. 2015;2015:563818. doi:10.1155/2015/563818
33. Cowman MK, Lee HG, Schwertfeger KL, McCarthy JB, Turley EA. The content and size of hyaluronan in biological fluids and tissues. *Front Immunol*. 2015;6:261. doi:10.3389/fimmu.2015.00261
34. Ke C, Wang D, Sun Y, Qiao D, Ye H, Zeng X. Immunostimulatory and antiangiogenic activities of low molecular weight hyaluronic acid. *Food Chem Toxicol*. 2013;58:401–407. doi:10.1016/j.fct.2013.05.032
35. Huang KY, Huang KY, Lew WZ, Fan KH, Chang WJ, Huang HM. Gamma-irradiation-prepared low molecular weight hyaluronic acid promotes skin wound healing. *Polymers*. 2019;11(7):1214. doi:10.3390/polym11071214
36. Zhong L, Liu Y, Xu L, et al. Exploring the relationship of hyaluronic acid molecular weight and active targeting efficiency for designing hyaluronic acid-modified nanoparticles. *Asian J Pharm*. 2019;14:521–530.
37. Mason TJ, Lorimer JP. *Applied Sonochemistry: The Uses of Power Ultrasound in Chemistry and Processing*. Weinheim: Wiley-VCH Verlag; 2002.
38. Bothner H, Waaler T, Wik O. Limiting viscosity number and weight average molecular weight of hyaluronate samples produced by heat degradation. *Int J Biol Macromol*. 1988;10(5):287–291. doi:10.1016/0141-8130(88)90006-2
39. Kim JK, Srinivasan P, Kim JH, et al. Structural and antioxidant properties of gamma irradiated hyaluronic acid. *Food Chem*. 2008;109(4):763–770. doi:10.1016/j.foodchem.2008.01.038
40. Sun S, Wang R, Huang Y, et al. Design of hierarchical beads for efficient label-free cell capture. *Small*. 2019;34(34):1902441. doi:10.1002/smll.201902441
41. Zhang H, Li J, Sun W, et al. Hyaluronic acid-modified magnetic iron oxide nanoparticles for MR imaging of surgically induced endometriosis model in rats. *PLoS One*. 2014;9(4):e94718. doi:10.1371/journal.pone.0094718
42. El-Dakdouki MH, El-Boubbou K, Zhu DC, Huang X. A simple method for the synthesis of hyaluronic acid coated magnetic nanoparticles for highly efficient cell labelling and in vivo imaging. *RSC Adv*. 2011;1(8):1449–1452. doi:10.1039/c1ra00737h
43. Wang HT, Chan YH, Feng SW, Lo YJ, Teng NC, Huang HM. Development and biocompatibility tests of electrospun poly-L-lactide nanofibrous membranes incorporating oleic acid-coated Fe3O4. *J Polymer Eng*. 2014;34(3):241–245. doi:10.1515/polyeng-2013-0206
44. Wu MP, Chang NC, Chung CL, et al. Analysis of titin in red and white muscles: crucial role on muscle contractions using a fish model. *BioMed Res Int*. 2018;5816875.
45. Kokesch-Himmelreich J, Schumacher M, Rohnke M, Gelinsky M, Janek J. ToF-SIMS analysis of osteoblast-like cells and their mineralized extracellular matrix on strontium enriched bone cements. *Biointerphases*. 2013;8(1):17. doi:10.1186/1559-4106-8-17
46. Pour MD, Ren L, Jennische E, Lange S, Ewing AG, Malmberg P. Mass spectrometry imaging as a novel approach to measure hippocampal $zinc^{+}$. *J Anal at Spectrom*. 2019;34(8):1581–1587. doi:10.1039/C9JA00199A
47. Lobsien D, Dreyer AY, Stroh A, Boltze J, Hoffmann KT. Imaging of VSOP labeled stem cells in agarose phantoms with susceptibility weighted and T2* weighted MR imaging at 3T: determination of the detection limit. *PLoS One*. 2013;8(5):e62644. doi:10.1371/journal.pone.0062644
48. Hamdous Y, Chebbi I, Mandawala C, et al. Biocompatible coated magnetosome minerals with various organization and cellular interaction properties induce cytotoxicity towards RG-2 and GL-261 glioma cells in the presence of an alternating magnetic field. *J Nanobiotechnology*. 2017;15(1):74. doi:10.1186/s12951-017-0293-2
49. Tiar QH, Suppiah DD, Julkapli NM. Fatty acid coated iron oxide nanoparticle: effect on stability, particle size and magnetic properties. *Colloids Surf a Physicochem Eng Asp*. 2020;606:125371. doi:10.1016/j.colsurfa.2020.125371
50. Alphandéry E, Abi-Haidar D, Seksek O, et al. Synthesized by magnetotactic bacteria, detecting fluorescence variations under dissociation of rhodamine B from magnetosomes following temperature, pH ghanges, or the application of radiation. *ACS Appl Mater Interfaces*. 2017;9(42):36561–36572. doi:10.1021/acsami.7b09720
51. Payne WM, Hill TK, Svechkarev D, Holmes MB, Sajja BR, Mohs AM. Multimodal imaging nanoparticles derived from hyaluronic acid for integrated preoperative and intraoperative cancer imaging. *Contrast Media Mol Imaging*. 2017;2017:9616791. doi:10.1155/2017/9616791
52. Cai H, An X, Cui J, et al. Facile hydrothermal synthesis and surface functionalization of polyethyleneimine-coated iron oxide nanoparticles for biomedical applications. *ACS Appl Mater Interfaces*. 2013;5(5):1722–1731. doi:10.1021/am302883m
53. Laith Z, Samarah AV. Mass spectrometry imaging based on laser desorption ionization from inorganic and nanophotonic platforms. *VIEW*. 2020;1(4):20200063. doi:10.1002/VIW.20200063
54. Shu W, Wang Y, Liu C, et al. Construction of a plasmonic chip for metabolic analysis in cervical cancer screening and evaluation. *Small Method*. 2020;4(4):1900469. doi:10.1002/smtd.201900469
55. Huang L, Wang L, Hu X, et al. Machine learning of serum metabolic patterns encodes early-stage lung adenocarcinoma. *Nat Commun*. 2020;11(1):3556. doi:10.1038/s41467-020-17347-6
56. Cao J, Shi X, Gurav DD, et al. Metabolic fingerprinting on synthetic alloys for medulloblastoma diagnosis and radiotherapy evaluation. *Adv Mater*. 2020;32(23):2000906. doi:10.1002/adma.202000906
57. Nygren H, Hagenhoff B, Malmberg P, Nilsson M, Richter K. Bioimaging TOF-SIMS: high resolution 3D imaging of single cells. *Microsc Res Tech*. 2007;70(11):969–974. doi:10.1002/jemt.20502
58. Alphandéry E. Nano-therapies for Glioblastoma treatment. *Cancers*. 2020;12(1):242. doi:10.3390/cancers12010242
59. Alphandéry E. Natural metallic nanoparticles for application in nano-oncology. *Int J Mol Sci*. 2020;21(12):4412. doi:10.3390/ijms21124412
60. Alphandéry E, Idbaih A, Adam C, et al. Biodegraded magnetosomes with reduced size and heating power maintain a persistent activity against intracranial U87-Luc mouse GBM tumors. *J Nanobiotechnology*. 2019;17(1):126. doi:10.1186/s12951-019-0555-2
61. Pinto A, Pocard M. Photodynamic therapy and photothermal therapy for the treatment of peritoneal metastasis: a systematic review. *Pleura Peritoneum*. 2018;18(3):20180124.